

Electronic structure of A-type antiferromagnetic LaMnO₃ by GW approximation

Y. Nohara¹, A. Yamasaki², S. Kobayashi³, and T. Fujiwara^{1,4}

¹ Department of Applied Physics, University of Tokyo, Tokyo 113-8656, Japan

² Max-Planck Institut für Festkörperforschung, Heisenbergstrasse 1, Stuttgart D-70569, Germany

³ Texas Instruments Japan Ltd., 6-24-1 Nishi-Shinjuku, Shinjuku-ku, Tokyo 160-8366, Japan

⁴ Core Research for Evolutional Science and Technology (CREST-JST), Japan Science and Technology Agency

(Dated: April 22, 2019)

The electronic structure of the A-type antiferromagnetic insulator LaMnO₃ is investigated by the GW approximation. The band gap and spectrum are in a good agreement with experimental observation. The on-site/off-site dynamical screened Coulomb interaction on Mn sites is also calculated. Comparison with the results by the Hartree-Fock and the static COHSEX approximations is discussed in detail. The dynamical screening effect is important for the band gap and widths.

PACS numbers: 71.10.-w, 71.15.-m, 71.20.-b

Transition metal oxides show particular characteristics of physical properties, especially large controllable change of properties with a small change of electron/hole doping or the external field. Among them, the hole-doped manganese oxides of perovskite structure, A_{1-x}B_xMnO₃ (A=La³⁺, Pr³⁺, Nd³⁺, ... and B=Ca²⁺, Sr²⁺, Ba²⁺, ...), have been paid much attention because of their properties, such as colossal magneto resistance (CMR), orbital, spin and charge order, metal-insulator transition and others. [1]

The starting material LaMnO₃ is A-type antiferromagnetic (A-AF) at low temperatures. The Mn³⁺ ion has t_{2g}³e_g¹ configuration, whose local spin quantum number $S=2$ caused by the Hund coupling. The atomic spin couples ferromagnetically with those of neighboring Mn ions on a same basal plane and couples antiferromagnetically with those of Mn ions on different planes. [2] The system shows the C-type orbital ordering with the Jahn-Teller (JT) distortion. [3]

The local spin density approximation (LSDA) is powerful tool to investigate the electronic structures. However, the LSDA sometimes does not give an overall picture of the electronic structures in transition metal compounds with strong correlation. In fact, the electronic structures of LaMnO₃ were calculated by the LSDA and the LSDA+U methods and these methods reveal several problems. For example, the LSDA underestimates the band gap and overestimates d-band width. [4] In the LSDA+U method, [5, 6] the Hubbard-type Coulomb interaction U is introduced so that the resultant band gap agrees with the observed optical gap. However, this method produces a strong bonding state with O-p and Mn-d orbitals in the deep valence region as an artifact.

The GW approximation (GWA) is a promising method for systems with electron-electron correlation but requires much heavier computational task. The GWA was applied to LaMnO₃ with a smaller unit cell in fictitious cubic paramagnetic phase, neglecting the JT distortion. [7] However, the JT distortion and tilted MnO₆ octahedra (GdFeO₃-type distortion) are crucially important in A-AF LaMnO₃. [8] The electronic structure of A-AF LaMnO₃ has not been calculated so far, because

the unit cell contains 20 atoms, *i.e.* 4 LaMnO₃, and large memory space and the parallel computation are needed.

In this letter, the electronic structure of the A-AF LaMnO₃ is investigated by the GWA, adopting the experimentally determined crystal structure of the orthorhombic *Pbnm* symmetry with the JT and the GdFeO₃-type distortion. [9] Present calculation is based on the Linear Muffin-Tin Orbital method with the Atomic Sphere Approximation (LMTO-ASA). [10] We use the 4×4×4 \mathbf{k} -mesh in the Brillouin zone and the resultant 30 \mathbf{k} -points in the irreducible zone. The set of the maximum orbital angular momentum of the LMTO basis in La, Mn, O and empty spheres are chosen to be (fddp). All E_ν 's for the LMTO linearization energy points are fixed at the averaged energies of occupied bands for respective orbital except La-p, for which E_ν is chosen in the unoccupied region.

The GWA is based on the many-body perturbation theory and is actually the first term approximation of the perturbation series for the one-body Green's function, [11] where the self-energy is replaced by the lowest order term of the expansion as $\Sigma = iGW$. Here G and W are the one-particle Green's function and the dynamically screened interaction, respectively. The dynamically screened interaction W in the GWA is treated by the random phase approximation (RPA) as

$$W = v + v\chi^0 W, \quad (1)$$

where v is the bare Coulomb interaction and χ^0 is the irreducible polarization function $\chi^0 = -iGG$.

We presume the wave-functions $\{\psi_{\mathbf{k}n}(\mathbf{r})\}$ of the LSDA to be reasonably good starting wave-functions, and then we adopt the LSDA Hamiltonian $H_0 = T + V^H + V_{\text{LSDA}}^{\text{xc}}$ as an unperturbed one. Here T is the kinetic energy, V^H is the Hartree potential, and $V_{\text{LSDA}}^{\text{xc}}$ is the exchange-correlation potential in the LSDA. The self-energy correction can be written with three terms as $\Delta\Sigma = \Sigma^x + \Sigma^c - V_{\text{LSDA}}^{\text{xc}}$, where $\Sigma^x (= iGv)$ is the exchange part (the Fock term) and $\Sigma^c (= iGW^c)$ is the dynamical correlation part. W^c is the second term in eq.(1). The Green's function is defined as

$$G = (E - H_0 - \Delta\Sigma)^{-1} \quad (2)$$

and the resultant quasiparticle energy is given as

$$E_{\mathbf{k}n} = \epsilon_{\mathbf{k}n} + Z_{\mathbf{k}n} \text{Re} \Delta \Sigma_{\mathbf{k}n}(\epsilon_{\mathbf{k}n}), \quad (3)$$

where $\epsilon_{\mathbf{k}n}$ is the LSDA eigen-energy. The self-energy is $\Delta \Sigma_{\mathbf{k}n}(\epsilon_{\mathbf{k}n}) = \langle \psi_{\mathbf{k}n} | \Sigma^x + \Sigma^c(\epsilon_{\mathbf{k}n}) - V_{\text{LSDA}}^{\text{xc}} | \psi_{\mathbf{k}n} \rangle$ and the renormalization factor is $Z_{\mathbf{k}n} = (1 - \partial \text{Re} \Delta \Sigma_{\mathbf{k}n}(\epsilon_{\mathbf{k}n}) / \partial E)^{-1}$. The renormalization factor $Z_{\mathbf{k}n}$ is an inverse effective mass ratio. In the present work we perform one-iteration calculation without self-consistency, *i.e.* $\Sigma = iG_0W_0$ and $\chi^0 = -iG_0G_0$.

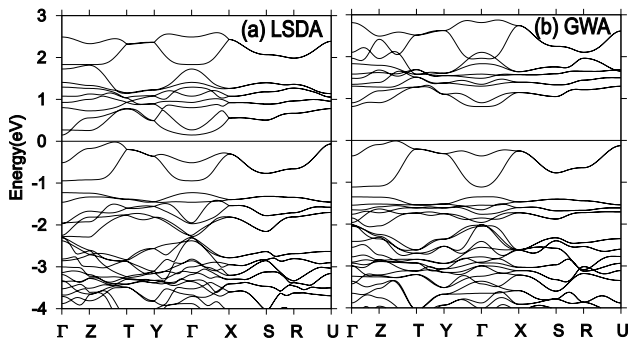


FIG. 1: Energy band of the A-AF LaMnO₃ by the LSDA (a), and by the GWA (b). The energy zero-th is fixed at the top of the respective valence band.

The important steps of our GWA are the offset method, [12] the product-basis set [13] and parallel computation. The offset method is essential to reproduce a response function with a small momentum transfer $\hbar\mathbf{k}$ and we use nearby 6 \mathbf{k} offset points $\frac{2\pi}{a}(\pm 0.0784 \times \frac{a}{b}, 0, 0)$, $\frac{2\pi}{b}(0, \pm 0.0784, 0)$, $\frac{2\pi}{c}(0, 0, \pm 0.0784 \times \frac{c}{b})$ instead of $\mathbf{k} = 0$, where a , b and c are the lattice constants in the orthorhombic system. In the calculation of the self-energy, a product of two spherical wave-functions $\phi\phi$ is expanded in terms of the new spherical functions called a product basis, whose total number is 1240 for the present choice. The product bases are specified by the total angular momentum of two wave-functions and we adopt the maximum total angular momentum of the product bases up to (fddp) for the calculation of Σ_c as the LMTO's themselves. This choice of total angular momentum reduces the number of the product bases to 700. See also refs.[14, 15].

The band structures calculated by (a) the LDA ($\epsilon_{\mathbf{k}n}$) and (b) the GWA ($E_{\mathbf{k}n}$) are shown in Figure 1. The band gap by the LSDA is as small as 0.16 eV and, on the other hand, that by the GWA becomes 0.82 eV, which agrees reasonably well with experimental optical gap 1.1 eV. [16] We can see that the width of the majority Mn-d(t_{2g}) band (in the energy region $-2.3 \text{ eV} \leq \epsilon_{\mathbf{k}n} \leq -1 \text{ eV}$ in the LSDA results) becomes narrower, and that of the majority Mn- $d_{3z^2-r^2}$ band (in the energy region $-1.0 \text{ eV} \leq \epsilon_{\mathbf{k}n} \leq 0 \text{ eV}$ in the LSDA results) becomes broader. The La-d and La-f bands appear in the LSDA calculation at the energy range of $3 \text{ eV} \leq \epsilon_{\mathbf{k}n} \leq 7.5 \text{ eV}$ above the top of the valence band. In the GWA, these

bands, La-d and La-f, are very strongly affected and shift to the energy range of $10 \text{ eV} \leq \epsilon_{\mathbf{k}n} \leq 15 \text{ eV}$. For the La-f, the band positions in the LSDA seem too low and also the LSDA Hamiltonian might not be a good starting point.

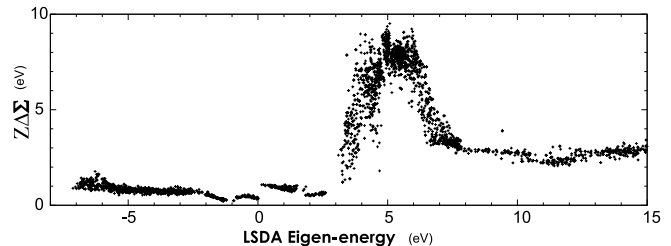


FIG. 2: The renormalized self-energy $Z_{\mathbf{k}n} \text{Re} \Delta \Sigma_{\mathbf{k}n}(\epsilon_{\mathbf{k}n})$ as a function of the LSDA eigen-energies $\epsilon_{\mathbf{k}n}$. The energy zero-th is fixed at the top of the LSDA valence band.

The renormalized self-energy $Z \text{Re} \Delta \Sigma$ is shown in Figure 2 as a function of the LSDA eigen-energy $\epsilon_{\mathbf{k}n}$. A step can be seen at $\epsilon_{\mathbf{k}n} = 0$ and it makes the band gap wider. In an energy region where $Z \text{Re} \Delta \Sigma$ is decreasing/increasing as a function of $\epsilon_{\mathbf{k}n}$, the width of these bands becomes narrower/broader. Thus, we find that, in the GWA, the O-p band in the energy range $-7.5 \text{ eV} \leq \epsilon_{\mathbf{k}n} \leq -2.5 \text{ eV}$ and the Mn-d(t_{2g}) band in the energy range $-2.5 \text{ eV} \leq \epsilon_{\mathbf{k}n} \leq -1.0 \text{ eV}$ become narrower. The reduction of the O-p band is attributed to that of hybridized Mn- t_{2g} component. The value of Z is around 0.6 in the Mn-d band region ($-2.5 \text{ eV} < E < 3.0 \text{ eV}$) and around 0.7 in the region of the O-p valence bands.

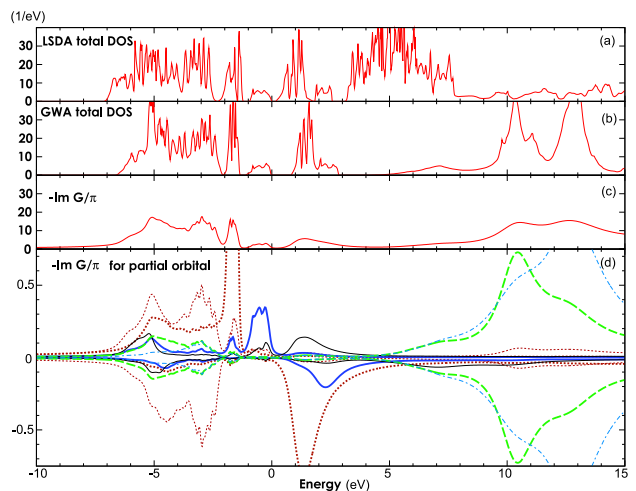


FIG. 3: (Color online) (a) Total DOS of the LSDA, (b) total DOS of the GW quasiparticles, and the imaginary part of the Green's function $-(1/\pi)\text{Im}G$ for (c) the total and (d) the partial components per one respective atom. In (d), the upper and the lower panels show the partial components with majority and minority spins, and bold solid line: Mn- $d_{3z^2-r^2}$, thin solid line: Mn- $d_{x^2-y^2}$, bold dotted line: Mn-d(t_{2g}), thin dotted line: O-p, bold chain line: La-d, dot-chain line: La-f. The energy zero-th in (a) is fixed at the top of the valence bands of the LSDA and in (b)~(d) at that of the GWA.

Figure 3 shows the density of states (DOS) or the imaginary part of the Green's function by the LSDA and the GWA. The band gap in the total DOS for the quasiparticle energy (b) is 0.82 eV. The imaginary part of the Green's function shows the smoothed and widely spread spectrum, because a quasiparticle has a finite lifetime. It should be noticed that the imaginary part of the Green's function gives an excellent agreement, except the La-d, with the observed XPS and XAS. [17]

In Figure 3(d), the notation of orbitals refers to the local coordinate. For example, $d_{3z^2-r^2}$ is the orbital along the longest Mn-O pair axis and $d_{x^2-y^2}$ on the perpendicular plane nearly along other Mn-O pair axes. The orbitals of $d(t_{2g})$ and $d(e_g)$ are split by the cubic crystal field and those of $d_{3z^2-r^2}$ and $d_{x^2-y^2}$ mainly by the JT distortion. The width for the valence bands does not change much and, on the other hand, that of the conduction bands becomes much broader. The partial Green's function is identical for all Mn ions, once one uses local orbitals in accordance with the local coordinates. This facts clearly show the characteristic orbital order (orbital C-type 'antiferro'-coupling) in LaMnO_3 ; *i.e.* each local orbital $d_{3z^2-r^2}$ aligns along the elongated Mn-O axis with antiferro- and ferro-coupling within and between basal planes, respectively.

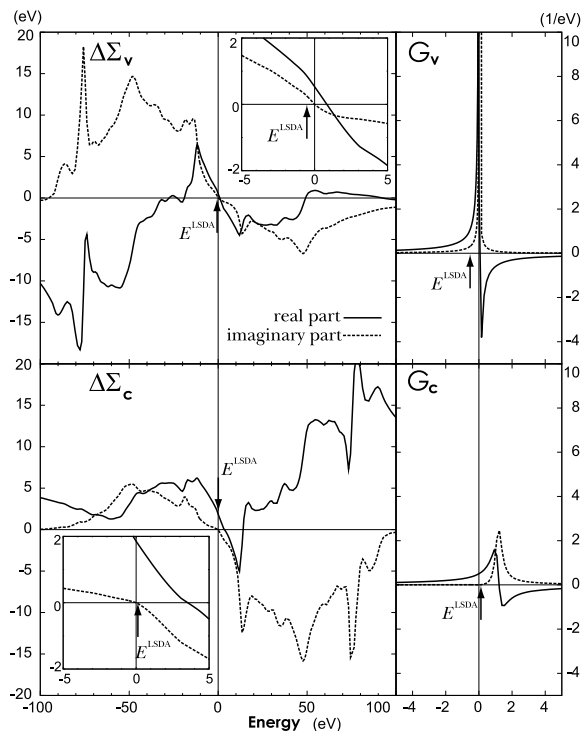


FIG. 4: The self-energy (left) and Green's function (right) of the highest valence (top) and lowest conduction (bottom) bands at $\mathbf{k} = 0$ (solid line: real part, dotted line: imaginary part). The energy zero-th is set at the top of the LSDA valence band. The inset shows the self-energy in a narrower energy range and the arrows indicate the position of the LSDA eigen-energies.

Figure 4 shows the self-energies and the Green's functions of the top of the valence band ($d_{3z^2-r^2}$) and the bottom of the conduction band (majority $d_{x^2-y^2}$ + minority $d(t_{2g})$) at Γ -point ($\mathbf{k} = 0$). Actually the overall feature of the self-energy is not very sensitive on the \mathbf{k} -points. One can notice the large difference of the shape of the Green's function; the one of the conduction band is much broader than that of the valence band. This fact is also confirmed for all deeper valence bands. The broadness of the Green's functions of the conduction bands is consistent to the behavior of the imaginary part of the self-energy. This fact is presumably attributed to the fact that the wave-functions of the conduction bands extent appreciably over the neighboring oxygen sites and are affected by strong polarization fluctuation.

The magnitude of the on-site/off-site d-d Coulomb interaction on Mn sites $\langle \phi_d \phi_d | W(E) | \phi_d \phi_d \rangle$ is shown in Figure 5. The off-site one is for a nearest-neighbor Mn pair on a basal plane (ferromagnetically coupling pair) and the other one for a nearest-neighbor Mn pair on different planes (antiferromagnetically coupling pair) is almost identical. The Coulomb interaction is strongly screened at low energies and is reduced to a few eV; 3.00 eV for on-site one with majority spins, 2.40 eV for on-site one with minority spins, 0.34 eV for off-site ones both with majority and minority spins. On the other hand, it approaches at the high energies to the values of bare ones 23.4 eV, 17.2 eV, 3.7 eV, respectively, because of no screening mechanism at high energy region.

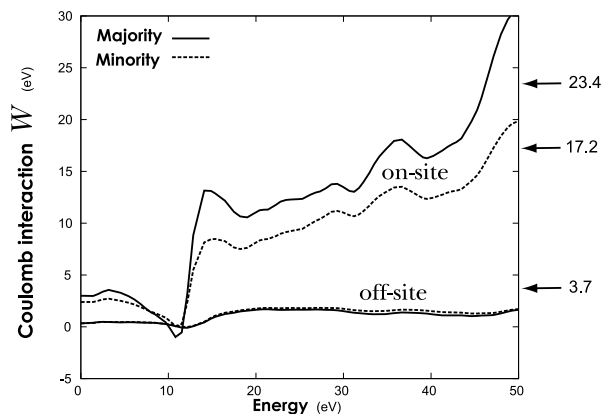


FIG. 5: The dynamical screened Coulomb interaction in LaMnO_3 (solid line: interaction with majority spins, dotted line: interaction with manority spins). The arrows indicate the extremum values at the higher energies.

The screening effects depend upon the excitation energy, since the electrons participating in the screening mechanism depend very much on their excitation energy. The screening for the on-site Coulomb interaction is quite efficient and this phenomena is attributed to the screening by easily mobile e_g electrons. [6] The $d(t_{2g})$ wave-functions is more localized than the LSDA picture and the width of the Mn- $d(t_{2g})$ bands becomes narrower as seen in Figure 1(b). The Coulomb interaction with minority spins is smaller than that with majority spins, be-

cause the radial wave-function $\phi_d(r)$ of minority spin has much components away from the core region and this fact results in a smaller values of a bare on-site Coulomb integral. It should be noticed that the screened Coulomb interaction is reduced to $W \simeq 0$ around $E \simeq 10$ eV in Figure 5. The excitation from O-p occupied states to La levels ($3 \sim 7.5$ eV) hybridized with Mn-d causes strong screening effects for Mn-d electrons. However, this large drop of the Coulomb interaction may be problematic, because the position of La-f bands may be too low in the LSDA calculation. Presumably, the large reduction of W in the energy region of La-f or La-d bands could be true but it should happen at higher energy region.

TABLE I: The band gap E_G , the band widths of occupied $d_{3z^2-r^2}$, $d(t_{2g})$ and O-p ($W_{3z^2-r^2}$, $W_{t_{2g}}$ and W_{Op}) and the magnetic moment $M(\mu_B)$. The band gap and widths are obtained from the calculated quasiparticle energy. The magnetic moments by the HFA, the COHSEX and the GWA are all the same.

	LDA	HFA	COHSEX	GWA	expt.
E_G (eV)	0.16	10.04	0.71	0.82	1.1 ^a
$W_{3z^2-r^2}$ (eV)	0.9	2.8	1.3	1.1	-
$W_{t_{2g}}$ (eV)	1.1	1.3	1.0	0.7	-
W_{Op} (eV)	4.8	5.4	5.4	4.6	-
$M(\mu_B)$	3.49				3.7 ^b , 3.87 ^c

^aRef. [16].

^bJ.B.A.A. Elemans, B. van Laar, K.R. van der Veen and B.O. Loopstra, J. Solid State Chem. **3**, 238 (1971).

^cRef. [9].

We summarize in Table 1 the calculated results for band gap, widths of occupied bands and magnetic moment with experimental results for comparison. The calculated results are for the LSDA, the Hartree-Fock approximation (HFA), the static COHSEX approximation (sCSA) [11] and the GWA. The sCSA is obtained with the self-energy of $E = 0$ or the zero excitation energy .

The band gap is found to be 0.82 eV by the GWA, which is in good agreement with experimental value 1.1 eV and slightly larger than the value by sCSA. The large band gap of the HFA is owing to the approximation free from the self-interaction. Then the sCSA adds the effect of the static screening. In fact, the change from the HFA to the cCSA is very large for the unoccupied Mn-d band. The dynamical part of the electron-electron interaction is attributed to the small difference between the band gaps of the sCSA and the GWA. The magnetic moment of magnetic insulators is not changed from the results of the LSDA in the HFA, the sCSA and the GWA, because these methods are the perturbative ones and we do not renew wave-functions. The band widths of Mn- $d_{3z^2-r^2}$ states by the GWA and the sCSA are slightly greater than that of the LSDA. The band width of Mn- $d(t_{2g})$ states by the GWA and the sCSA are less than that of the LSDA. The band width of O-p bands by GWA is less than the LSDA value. These results of the band widths indicate the wave-functions of Mn- $d(t_{2g})$ and O-p states becomes more localized by the GWA and that of Mn- $d(e_g)$ less. Therefore, the screening effect affects to $d(t_{2g})$ and $d(e_g)$ states in an opposite way.

In summary, we applied the GWA to the A-type anti-ferromagnetic LaMnO₃. Band gap and magnetic moment are in good agreement with experimental results. The band width of Mn majority $d(t_{2g})$ states become narrower due to the correlation effect and, on the contrary, that of Mn majority $d_{3z^2-r^2}$ states becomes broader. The spectrum shows an excellent agreement with experimental results. We also present the energy depending Coulomb interaction, and find that on-site d-d Coulomb interaction is strongly screened at the low energy region due to mobile e_g electrons.

Computation was partially carried out by use of the facilities at the Supercomputer Center, Institute for Solid State Physics, University of Tokyo, and the Institute of Molecular Science at Okazaki.

-
- [1] Y.Tokura, Physics Today, **56**, 50 (2003).
[2] E.O.Wollan and W.C.Koehler, Phys. Rev. **100**, 545 (1955).
[3] K.I.Kugel and D.I.Khomskii, Sov. Phys. Usp. **25**, 231 (1982).
[4] W.E.Pickett and D.J.Singh, Phys. Rev. **B53**, 1146 (1996).
[5] S.Satpathy Z.S.Popović and F.R.Vukajlović, Phys. Rev. Lett. **76**, 960 (1996).
[6] I.Solovyev, N.Hamada and K.Terakura, Phys. Rev. **B53**, 7158 (1996).
[7] H.Kino, F.Aryasetiawan, I.Solovyev, T.Miyake, T.Ohno and K.Terakura, Physica **B329-333**, 858 (2003).
[8] I.Solovyev, N.Hamada and K.Terakura, Phys. Rev. Lett. **76**, 4825 (1996).
[9] F.Moussa, M.Hennion, J.Rodriguez-Carvajal, H.Moïdden, LPinsard and A.Revcolevschi, Phys. Rev. **B54**, 15149 (1996).
[10] O.K.Andersen, Phys. Rev. **B12**, 3060 (1975).
[11] L.Hedin, Phys. Rev. **139**, A796 (1965).
[12] T.Kotani and M.van Schilfhaarde, private communications.
[13] F.Aryasetiawan and O.Gunnarsson, Phys. Rev. **B49**, 16214 (1994).
[14] A.Yamasaki and T.Fujiwara, Phys. Rev. **B66**, 245108 (2002).
[15] A.Yamasaki and T.Fujiwara, J. Phys. Soc. Jpn. **72**, 607 (2003).
[16] T.Arima, Y.Tokura and J.B.Torrance, Phys. Rev. **B48**, 17006 (1993).
[17] T.Saitoh, A.E.Bocquet, T.Mizokawa, H.Namatame, A.Fujimori, M.Abbate, Y.Takeda and M.Takano, Phys.

Rev. B51, 13942 (1995).